Turkish Journal of Electrical Engineering & Computer Sciences

http://journals.tubitak.gov.tr/elektrik/

Research Article

Turk J Elec Eng & Comp Sci
(2022) 30: 785 – 804
© TÜBİTAK
doi:10.3906/elk-2106-134

Robust position/force control of nonholonomic mobile manipulator for constrained motion on surface in task space

Gülin ELİBOL SEÇİL[1,*], **Serhat OBUZ**[1,2], **Osman PARLAKTUNA**[1,3]
Department of Electrical and Electronics Engineering, Faculty of Engineering and Architecture,
Eskisehir Osmangazi University, Eskisehir, 26040, Turkey

Received: 25.06.2021 • **Accepted/Published Online:** 31.10.2021 • **Final Version:** 21.03.2022

Abstract: In this paper, a robust controller is developed for a mobile manipulator (MM) to track reference position/force trajectories. Nonholonomic and holonomic constraints are considered for the mobile platform and manipulator, respectively. Additionally, the control design considers the uncertainties in parameters of the dynamics of the mobile manipulator with a bounded time varying additive disturbance (unmodelled effects, external disturbances). A Lyapunov-based stability analysis is used to prove semiglobal uniform ultimate boundedness of the tracking error signals and the position/force of the system track to an arbitrarily small neighborhood of the reference trajectories. Numerical results for a mobile manipulator, which is formed from a differential drive mobile platform and 2 DOF Revolute-Revolute (RR) manipulator, show that the position of the end-effector and the applied force track the desired position and the force trajectories, respectively.

Key words: Mobile manipulator, position/force control, constrained motion, robust controller, Gazebo Simulation

1. Introduction

The literature on designing controllers of the position/force control for the robot manipulators (RMs) and position control for the mobile robots (MRs) have been presented with various approaches. The control design for the RM is challenging since its dynamics include some complexities such as nonlinear terms [1], friction forces [2], uncertainties [2, 3]. In order to provide position/force tracking for the RMs, feedback linearization based controllers [4, 5], adaptive controllers [6–9], neural network (NN) based controllers [1, 2] and robust controller [3] are proposed. The techniques used in [4, 5] require exactly/partially known RM dynamics and the works in [6–9] assumed that the dynamic model of RMs is linearly parameterizable. However, the obligations of the proposed controllers in [4–9] might not be fulfilled in practice. Furthermore, the position tracking for MRs is problematic due to included nonholonomic constraints [10–14]. A backstepping-like feedback linearization approach [10], an adaptive controller with the velocity/acceleration limiter [11], a NN based controller [13], a sliding mode robust controller [14], a differentiable kinematic controller [12] and a robust kinematic controller [15], were designed for position tracking of the MRs.

Mobile manipulators (MM) are robotic systems composed of mounted RMs onto mobile platforms (MPs). For many tasks, the end-effector contacts surfaces of objects, and a force arises between the end-effector and surface; therefore, many robotic operations require force tracking together with position tracking. Industrial

*Correspondence: gelibol@ogu.edu.tr

This work is licensed under a Creative Commons Attribution 4.0 International License.

mobile manipulators, which are formed of industrial manipulators and mobile platforms, such as ABBY, Little Helper, OMNIVIL, etc., perform many tasks in industrial environments semiautonomously or autonomously [16–20]. The position/force control is needed during pick-place [18], object handling [21], sealant [22] tasks for applications of industrial mobile manipulation. The position and force control of MMs is challenging due to the dynamic of the MM is nonlinear [23] and includes structural and nonstructural uncertainties [24]. Furthermore, the RM and the MP have a coupled structure. Designing a controller for both systems concurrently is a challenging problem due to the coupled structure. Another difficulty for designing a controller for MMs arises from holonomic constraints (e.g., as the task constraints and the structure of the RM) and nonholonomic constraints restricting the motion of the MR [25]. Few studies have focused on designing a controller for MMs to simultaneously provide position and force tracking [24, 26–29]. In [24], a controller is developed to track the reference position/force trajectories for a MM with both nonholonomic and holonomic constraints. In [30], an NN-based extension attached to a model-based controller is designed to track the reference position and force of an MM in the presence of uncertainties and disturbances. The control designs in [24, 30] require the exact model of the dynamics of the MM. In [29], an adaptive controller is designed for MM with holonomic and nonholonomic constraints to ensure force/position tracking despite the uncertainties and disturbances in its dynamic. In [27], the holonomic constraint for the nonholonomic MM is assumed to be uncertain and the proposed adaptive controller provides position/force tracking despite uncertain parameters and disturbances in the dynamic. In [28], an output-feedback control is realized for the holonomic constrained nonholonomic MMs to provide position/force tracking. In [31] a backstepping-based adaptive controller is utilized for the constrained MM for tracking reference position/force trajectories. The aforementioned works in [27, 29, 31, 32] ensure position/force control tracking for MM assuming that the dynamics of the MMs are linearly parameterized with uncertainties. However, the dynamics of the MMs might be nonlinearly parameterized with uncertainties in some applications, especially the dynamic of friction may not hold this condition all the time [32]. To overcome the requirement of the linearly parameterizable condition in the dynamic, very few controllers were designed in relevant literature [33]. However, the stability result for the presented controller in [33] is local. Realizing the gap in the extant literature, more research is needed for designing a robust controller to ensure the position and force tracking despite the holonomic/nonholonomic constraints, uncertainties, and disturbances in the dynamic of MMs.

In this paper, a novel robust position/force controller is developed for a mobile manipulator that has coupled structure, uncertainties in the dynamic and an unknown time varying disturbance. Moreover, the mobile manipulator has both holonomic and nonholonomic constraints. It is assumed that the force measurement of the end-effector of MM on task space is available as in [34]. The designed controller does not require any linearization technique or the linearly parameterizable assumption for the MMs dynamic, unlike proposed controllers in [24, 27, 29–31]. Furthermore, the controller in [24, 30] needs the exact knowledge of the dynamic model of MM, however, in this paper, the robust controller is designed to track the position/force of MM without the requirements of an exact model of the mobile manipulator. The controller in [24] does not consider the disturbances in the dynamic; however, for real-time applications, most of the dynamics are subject to disturbances. The designed controller is robust to additive unknown time varying disturbances in the dynamics. The designed controller is applicable for the constrained/unconstrained motion, unlike the controllers in [24, 27, 29]. A PID-based (proportional-integral-derivative based) continuous robust controller is developed to increase the robustness of the controller under the uncertainties and disturbances and to

improve the position/force tracking performance. The simulations on MATLAB-Simulink and ROS-Gazebo are performed under realistic constraints to show the performance of the controller. The designed robust controller ensures semiglobal uniformly ultimately bounded tracking error signals for the position and force trajectories. A Lyapunov-based stability analysis is used to verify that the position/force of the system track to an arbitrarily small neighborhood of the reference trajectories. Numerical results show that the position of the end-effector and the applied force track the reference position and the force trajectories. Explanations of all abbreviations are given in Table 1 in Appendix A.

2. Dynamics of the mobile manipulator

The dynamic model of the constrained MM, which includes nonholonomic constraints in the MP and holonomic constraints in the RM, is expressed in the generalized coordinates as [35]

$$M(q)\ddot{q}+C(q,\dot{q})\dot{q}+N(q,\dot{q})+d(t)=B(q)\tau(t)+f(t), \tag{1}$$

where $q \triangleq [\, q_v^T \quad q_a^T \,]^T \in \mathbb{R}^n$ symbolizes the position vector of the MM, $\dot{q}, \ddot{q} \in \mathbb{R}^n$ are the velocity and acceleration vectors of the MM, respectively. The generalized coordinates of the position of the MP and the RM are denoted by $q_v \in \mathbb{R}^m$ and $q_a \in \mathbb{R}^k$, respectively. The inertia matrix of the MM is symbolized as $M(q) \triangleq \begin{bmatrix} M_v & M_{va} \\ M_{av} & M_a \end{bmatrix} \in \mathbb{R}^{n\times n}$. The centripetal and Coriolis forces of the MM are denoted as $C(q,\dot{q}) \triangleq \begin{bmatrix} C_v & C_{va} \\ C_{av} & C_a \end{bmatrix} \in \mathbb{R}^{n\times n}$. The vector $N(q,\dot{q}) \triangleq \left[N_v^T \; N_a^T\right]^T \in \mathbb{R}^n$ includes the dynamics of the gravity $G(q) \in \mathbb{R}^n$, static/dynamic friction $F(\dot{q}) \in \mathbb{R}^n$ of the MM. The unknown time varying bounded additive disturbance is denoted as $d(t) \triangleq [d_v^T \; d_a^T]^T \in \mathbb{R}^n$ and the transformation matrix of the MM's input is denoted as $B(q) \triangleq \begin{bmatrix} B_v & 0_{m\times k} \\ 0_{k\times w} & B_a \end{bmatrix} \in \mathbb{R}^{n\times(w+k)}$ where $w \in \mathbb{R}$ is the number of driven wheels of the MP. The torque of the MM is defined as $\tau(t) \triangleq \left[\tau_v^T \; \tau_a^T\right]^T \in \mathbb{R}^{(w+k)}$ and the constraint force vector is denoted as $f(t) \triangleq [\, f_n^T \quad f_h^T \,]^T \in \mathbb{R}^n$. Furthermore, the detailed explanations of the matrices of the dynamic model are given in Table 2 and the control input and the subsequent developments depend on the following assumptions and properties.

Assumption 1 *The mobile platform is assumed to be nonslippage [25].*

Assumption 2 *The unknown time varying additive disturbance $d(t)$ is assumed to have an upper bound, which is constant and known [36, 37].*

Remark 1 *The additive disturbance $d(t)$ includes both parametric uncertainties and unmodeled effects ($d_{\Delta_{unc}}(t) \in \mathbb{R}^n$), and external disturbances ($d_{ext}(t) \in \mathbb{R}^n$).*

$$d(t) = d_{ext}(t) + d_{\Delta_{unc}}(t),$$

It should be noted that the designed control signal in this paper does not in need of the exact knowledge of $M(q)$, $C(q,\dot{q})$, $G(q)$, and $F(\dot{q})$. The aforementioned matrices and vectors in (1) may include some uncertainties, which are denoted as $M_{unc} \in \mathbb{R}^{n\times n}, C_{unc} \in \mathbb{R}^{n\times n}, G_{unc} \in \mathbb{R}^n$ and $F_{unc} \in \mathbb{R}^n$, and are used in the simulation to show the robustness of the controller under the added parametric uncertainties, unmodelled effects, and external disturbances.

Property 1 *The inertia matrix $M(q)$ is a positive definite, symmetric matrix and satisfies the following property [38].*

$$\underline{m}||x||^2 \leq x^T M(q)x \leq \overline{m}||x||^2, \ \ \forall x \in \mathbb{R}^n,$$

where $\underline{m}, \overline{m} \in \mathbb{R}_{>0}$ are known constants.

Property 2 *The inertia matrix $M(q)$ and the centripetal and Coriolis forces $C(q,\dot{q})$ satisfy the skew symmetry property [38].*

Assumption 3 *The matrices $M(q)$, $C(q,\dot{q})$, $N(q,\dot{q})$ and $B(q)$, along with their first order partial derivatives, are assumed to have bounds provided that the functions $q, \dot{q}, \ddot{q}$ are bounded [39].*

Using (1), the dynamics of the mobile platform and manipulator is written as

$$M_v\ddot{q}_v + M_{va}\ddot{q}_a + C_v\dot{q}_v + C_{va}\dot{q}_a + N_v + d_v(t) = B_v\tau_v + f_n, \tag{2}$$

$$M_{av}\ddot{q}_v + M_a\ddot{q}_a + C_{av}\dot{q}_v + C_a\dot{q}_a + N_a + d_a(t) = B_a\tau_a + f_h. \tag{3}$$

The nonholonomic constraint exists due to the mechanical structure of the MP and causes restrictions on velocities. Such velocity constraints restrict the motion of the platform. Therefore, the velocity constraints must be satisfied during the motion of the MP. In order to fulfill nonholonomic constraint conditions and eliminate the nonholonomic constraint forces, the MM is needed to be written in terms of the generalized combined joint-space coordinates.

2.1. Combined joint-space dynamic model of mobile manipulator

The MP has $c_n \in \mathbb{R}_{>0}$ nonholonomic constraints which exist due to wheels of the platform and restrict MP to move along the lateral direction [25, 40]. The constraints restrict the motion of the MP by limiting the sets of state trajectories and are always fulfilled via nonholonomic constraint forces [41]. The nonholonomic constraints of the MP can be defined in Pfaffian form as $A_v(q_v)\,\dot{q}_v = 0_{c_n}$ where $A_v : \mathbb{R}^m \to \mathbb{R}^{c_n \times m}$ is the kinematic constraint matrix. The nonholonomic constraints forces can be defined as $f_n = A_v^T(q_v)\,\lambda_n$, where $\lambda_n \in \mathbb{R}^{c_n}$ is the Lagrangian multiplier of the nonholonomic constraints. There exists a set of smooth and linearly independent vector fields, $S_v(q_v) \in \mathbb{R}^{m \times w}$, spanning the null space of $A(q_v)$ and is defined as

$$S_v^T(q_v)\,A_v^T(q_v) = 0_{w \times c_n}. \tag{4}$$

An auxiliary velocity vector $\dot{\theta}_v \triangleq [\dot{\theta}_L \ \ \dot{\theta}_R] \in \mathbb{R}^w$, where $\dot{\theta}_R, \dot{\theta}_L \in \mathbb{R}$ are the angular velocities of right and left wheels of the MP, satisfies the following property:

$$\dot{q}_v = S_v(q_v)\,\dot{\theta}_v. \tag{5}$$

Multiplying both sides of (2) by $S_v^T(q_v)$ then substituting (5) and the time derivative of (5) into (2) and (3), the dynamics given in (1) can be transformed into the combined joint-space of the MM as

$$M_j\ddot{\theta}_j + C_j\dot{\theta}_j + N_j + d_j = B_j\tau + f_j, \tag{6}$$

where $\theta_j \triangleq \begin{bmatrix} \theta_v^T & q_a^T \end{bmatrix}^T \in \mathbb{R}^{w+k}$ is the position vector, $\dot{\theta}_j, \ddot{\theta}_j \in \mathbb{R}^{w+k}$ are the velocity and acceleration of the MM in combined joint-space, respectively, $M_j \triangleq \begin{bmatrix} S_v^T M_v S_v & S_v^T M_{va} \\ M_{av} S_v & M_a \end{bmatrix} \in \mathbb{R}^{(w+k)\times(w+k)}$, $N_j \triangleq \begin{bmatrix} S_v^T N_v \\ N_a \end{bmatrix} \in \mathbb{R}^{(w+k)}$, $C_j \triangleq \begin{bmatrix} S_v^T \left(C_v S_v + M_v \dot{S}_v\right) & S_v^T C_{va} \\ M_{av}\dot{S}_v + C_{av} S_v & C_a \end{bmatrix} \in \mathbb{R}^{(w+k)\times(w+k)}$, $d_j \triangleq \begin{bmatrix} S_v^T d_v \\ d_a \end{bmatrix} \in \mathbb{R}^{(w+k)}$, $B_j \triangleq \begin{bmatrix} S_v^T B_v & 0_{w\times k} \\ 0_{k\times w} & B_a \end{bmatrix} \in \mathbb{R}^{(w+k)\times(w+k)}$, $f_j \triangleq \begin{bmatrix} 0 \\ f_h \end{bmatrix} \in \mathbb{R}^{(w+k)}$. Consequently, the nonholonomic constraint force is eliminated and the motion of the MP is restricted. The force between the surface and the end-effector is measured in task space; therefore, the dynamic model in combined joint-space coordinates needs to be transformed to the task space of the MM.

2.2. Task space dynamic model of mobile manipulator

The relationship between the velocity of the end-effector according to the combined joint-space and the task space is defined as:

$$\dot{X}_T = J_{jt}\dot{\theta}_j, \tag{7}$$

where $X_T, \dot{X}_T \in \mathbb{R}^{c_t}$ are the position and the velocity of the end-effector in task space, respectively and $J_{jt} \in \mathbb{R}^{c_t\times(w+k)}$ is the Jacobian matrix, where $c_t \in \mathbb{R}_{>0}$ is the number of variables in the task space. Using (7), the velocity and acceleration of the MM in combined joint-space can be defined in the task space as

$$\dot{\theta}_j = J_{jt}^{\dagger}\dot{X}_T, \qquad \ddot{\theta}_j = -J_{jt}^{\dagger}\dot{J}_{jt}J_{jt}^{\dagger}\dot{X}_T + J_{jt}^{\dagger}\ddot{X}_T, \tag{8}$$

where $J_{jt}^{\dagger} \in \mathbb{R}^{(w+k)\times c_t}$ is the pseudo-inverse of the J_{jt}, $\ddot{X}_T \in \mathbb{R}^{c_t}$ is the acceleration of the end-effector in the task space. Using (8), the combined joint-space dynamics in (6) is transformed to the task space and the nonholonomic constraints are eliminated as

$$M_T\ddot{X}_T + C_T\dot{X}_T + N_T + d_T = B_T\tau + f_T, \tag{9}$$

where $M_T \triangleq \left(J_{jt}^{\dagger}\right)^T M_j J_{jt}^{\dagger} \in \mathbb{R}^{c_t\times c_t}$, $C_T \triangleq \left(J_{jt}^{\dagger}\right)^T \left(C_j - M_j J_{jt}^{\dagger}\dot{J}_{jt}\right) J_{jt}^{\dagger} \in \mathbb{R}^{c_t\times c_t}$, $N_T \triangleq \left(J_{jt}^{\dagger}\right)^T N_j \in \mathbb{R}^{c_t}$, $d_T \triangleq \left(J_{jt}^{\dagger}\right)^T d_j \in \mathbb{R}^{c_t}$, $B_T \triangleq \left(J_{jt}^{\dagger}\right)^T B_j \in \mathbb{R}^{c_t\times(w+k)}$ and $f_T \triangleq \left(J_{jt}^{\dagger}\right)^T f_j \in \mathbb{R}^{c_t}$. Designing control signal to provide tracking for position and force simultaneously is challenging since the control input signals for both position and force are coupled in the task space model. To overcome the difficulty of the control design, it may be advantageous to use the reduced order dynamic model given in [42].

2.3. Reduced order dynamic model of the mobile manipulator

The holonomic constraint, which is existed due to the desired task, for the end-effector of the MM can be defined as a restriction of the dynamics on the constraint manifold as

$$\Omega_h \triangleq \{(X_T, \dot{X}_T) | \Theta(X_T) = 0_{c_h},\ A_a(X_T)\dot{X}_T = 0_{c_h}\}, \tag{10}$$

where $\Theta : \mathbb{R}^{c_t} \to \mathbb{R}^{c_h}$ and its null space defines the holonomic constraint of MM such that $\Theta(X_T) = 0_{c_h}$ and $c_h \in \mathbb{R}_{>0}$ is the number of holonomic constraints. There exists a holonomic constraint matrix, $A_a \in \mathbb{R}^{c_h\times c_t}$, that is defined as

$$A_a(X_T) \triangleq \frac{\partial\Theta(X_T)}{\partial X_T}. \tag{11}$$

Assumption 4 *The holonomic constraints of the end-effector are assumed to be known exactly and frictionless [9].*

Assumption 5 *The matrix* $A_a(X_T)$ *can be separated as* $A_a = \left[\frac{\partial \Theta(X_T)}{\partial x_1} \in \mathbb{R}^{c_h \times c_t - c_h} \;\; \frac{\partial \Theta(X_T)}{\partial x_2} \in \mathbb{R}^{c_h \times c_h}\right]$ *and the* $x_2 \in \mathbb{R}^{c_h}$ *should be selected to ensure that* $\frac{\partial \Theta(X_T)}{\partial x_2}$ *is full rank [9].*

The task space variables can be partitioned as $X_T = \left[x_1^T \;\; x_2^T\right]^T$, where $x_1 \in \mathbb{R}^{c_t - c_h}$ denotes the unconstrained task space variables and $x_2 \in \mathbb{R}^{c_h}$ is a function of the holonomic constraints of the MM in the task space. Using Assumption 5 and the Implicit Function Theorem, there exists a unique function $\Omega : \mathbb{R}^{c_t - c_h} \to \mathbb{R}^{c_h}$ on the constraint surface such that $x_2 = \Omega(x_1)$. The constraint function can be rewritten as $\Theta(X_T) \triangleq \Theta(x_1, x_2) = \Theta(x_1, \Omega(x_1)) = 0_{c_h}$ [9]. To define the reduced order dynamic model, the variables $u_1 \in \mathbb{R}^{c_t - c_h}$ and $u_2 \in \mathbb{R}^{c_h}$ are defined as

$$u \triangleq \begin{bmatrix} u_1 \\ u_2 \end{bmatrix} = \begin{bmatrix} x_1 \\ x_2 - \Omega(x_1) \end{bmatrix}. \tag{12}$$

where u is defined using the position of the end-effector in the task space and the holonomic constraint. Using (12), the relation between the states of the task space and the reduced order model becomes:

$$\dot{X}_T = T\dot{u}, \qquad \ddot{X}_T = \dot{T}\dot{u} + T\ddot{u}, \tag{13}$$

where $T \in \mathbb{R}^{c_t \times c_t}$ is the transformation matrix. Substituting (13) into (9), multiplying both sides by T^T and using $f_T = \left(J_{jt}^{\dagger}\right)^T f_j = A_a^T \lambda_h$, where $\lambda_h \in \mathbb{R}^{c_h}$ is the Lagrangian multiplier of holonomic constraints, the reduced order dynamic model for the constrained MM is obtained as

$$M_{ST}\ddot{u} + C_{ST}\dot{u} + N_{ST} + d_{ST} = B_{ST}\tau + (A_a T)^T \lambda_h, \tag{14}$$

where $M_{ST} \triangleq T^T M_T T \in \mathbb{R}^{c_t \times c_t}$, $C_{ST} \triangleq \left(T^T M_T \dot{T} + T^T C_T T\right) \in \mathbb{R}^{c_t \times c_t}$, $N_{ST} \triangleq T^T N_T \in \mathbb{R}^{c_t}$, $d_{ST} \triangleq T^T d_T \in \mathbb{R}^{c_t}$, $B_{ST} \triangleq T^T B_T \in \mathbb{R}^{c_t \times (w+k)}$.

3. Control development

The objective is to design a controller that enables the end-effector of the MM to track the desired position and force trajectories despite uncertainties in the dynamic model subjected to additive disturbances. To quantify the control objective, a measurable error signal for position tracking $e_0 \in \mathbb{R}^{c_t}$ and an auxiliary tracking error $e_1 \in \mathbb{R}^{c_t}$ are defined as

$$e_0 \triangleq \int_{t_0}^{t} (u_d(\xi) - u(\xi)) d\xi, \tag{15}$$

$$e_1 \triangleq \dot{e}_0 + \alpha_1 e_0, \tag{16}$$

where $u_d \in \mathbb{R}^{c_t}$ is the desired position trajectory and $\alpha_1 \in \mathbb{R}^{c_t \times c_t}$ is an adjustable, positive definite, diagonal (APDD) control gain matrix. The time derivative of (15) defines the error between desired and actual position of the end-effector.

Assumption 6 *The desired position trajectory* $u_d \in \mathbb{R}^{c_t}$ *and its first and second time derivatives* $\dot{u}_d, \ddot{u}_d \in \mathbb{R}^{c_t}$, *and the desired force trajectory* $\lambda_d \in \mathbb{R}^{c_h}$ *are bounded by constants which are known [43].*

To facilitate the control development, an auxiliary signal $r \in \mathbb{R}^{c_t}$ is defined as

$$r \triangleq \dot{e}_1 + \alpha_2 e_1, \tag{17}$$

where $\alpha_2 \in \mathbb{R}^{c_t \times c_t}$ is an APDD control gain matrix. Multiplying both sides of the time derivative of (17) by M_{ST}, using (14)-(17), the open-loop dynamics for r is obtained as

$$M_{ST}\dot{r} = \tilde{N} + N_d - B_{ST}\tau - (A_a T)^T \lambda_h - e_1, \tag{18}$$

where $\tilde{N}, N_d \in \mathbb{R}^{c_t}$ are defined as

$$\begin{aligned} \tilde{N} \triangleq\ & M_{ST}(u)\left(\ddot{u}_d + (\alpha_1+\alpha_2)\ddot{e}_0 + (\alpha_2\alpha_1)\dot{e}_0\right) + C_{ST}\left(u, \dot{u}\right)\left(\dot{u}_d + (\alpha_1+\alpha_2)\dot{e}_0 + (\alpha_2\alpha_1)e_0\right) \\ & + d_{ST}(t) + N_{ST}(u, \dot{u}) + e_1 - M_{ST}(u_d)\ddot{u}_d - C_{ST}\left(u_d, \dot{u}_d\right)\dot{u}_d - N_{ST}(u_d, \dot{u}_d) - d_{ST}(t), \\ N_d \triangleq\ & M_{ST}(u_d)\ddot{u}_d + C_{ST}(u_d, \dot{u}_d)\,\dot{u}_d + N_{ST}(u_d, \dot{u}_d) + d_{ST}(t). \end{aligned} \tag{19}$$

Remark 2 *Based on Assumptions 3 and 6, the Mean-Value Theorem can be utilized to acquire an upper bound for* $\tilde{N}$ *as in [34]*

$$\left\|\tilde{N}\right\| \leq \rho\left(\|z\|\right)\|z\|, \tag{20}$$

where $z \triangleq [e_0^T\ e_1^T\ r^T]^T \in \mathbb{R}^{3c_t}$ *and* $\rho : [0, \infty) \to [0, \infty)$ *is a radially unbounded, positive definite, and strictly increasing function.*

Remark 3 *Based on Assumptions 2, 3, and 6 , the following upper bound can be obtained for* N_d *as*

$$\|N_d\| \leq \bar{N}_d, \tag{21}$$

where $\bar{N}_d \in \mathbb{R}_{>0}$ *is a known constant.*

According to the stability analysis, the control signal is designed for position and force tracking as

$$\tau \triangleq B_{ST}^{\dagger}(kr + \tau_f), \tag{22}$$

where $k \in \mathbb{R}^{c_t \times c_t}$ is an APDD control gain matrix and the force control input signal $\tau_f \in \mathbb{R}^{c_t}$ is designed as

$$\tau_f \triangleq -(A_a T)^T \lambda_c, \tag{23}$$

where $\lambda_c \in \mathbb{R}^{c_h}$ is the force control vector and designed as

$$\lambda_c \triangleq \lambda_d + K_\lambda e_\lambda, \tag{24}$$

where $K_\lambda \in \mathbb{R}^{c_h \times c_h}$ is an APDD control gain matrix and $e_\lambda \in \mathbb{R}^{c_h}$ denotes the error between the desired and measured force, e_λ is defined as

$$e_\lambda \triangleq \lambda_d - \lambda_h. \tag{25}$$

Substituting the control signal (22) and (23) into (18), the closed-loop dynamics for r is obtained as

$$M_{ST}\dot{r} = \tilde{N} + N_d - (kr - (A_a T)^T \lambda_c) - (A_a T)^T \lambda_h - e_1. \tag{26}$$

Remark 4 *Using (24) and (25), the following expression is obtained as [43]*

$$e_\lambda = \frac{\lambda_c - \lambda_h}{(1 + K_\lambda)}. \tag{27}$$

Using (18)-(22), $\lambda_c - \lambda_h$ *can be defined with a function* $\zeta\left(\int_0^t u(\xi)d\xi, \int_0^t u_d(\xi)d\xi, u, u_d, \dot{u}, \dot{u}_d, \ddot{u}_d\right) \in \mathbb{R}$ *that depends the position and velocity of the MM and its desired trajectories. It should be noted that as* K_λ *is increased, the error between the desired and actual force will be reduced.*

Theorem 1 *Given the dynamics in (1), the controller given in (22)-(23) ensures semiglobally, uniformly, ultimately boundedness of the tracking error signals in sense that*

$$\limsup_{t\to\infty} \|u_d - u\| \leq \epsilon_1 exp\left(-\epsilon_2 \left(t - t_0\right)\right) + \epsilon_3, \tag{28}$$

where $\epsilon_1, \epsilon_2, \epsilon_3 \in \mathbb{R}_{>0}$ *are known constants. The control gain* k *must satisfy the following gain condition*

$$k_{min} \geq \frac{2\rho^2\left(\|z\left(t_0\right)\|\right)}{\min\left\{\left(\alpha_{1min} - \frac{1}{2}\right), \left(\alpha_{2min} - \frac{1}{2}\right), \frac{k_{min}}{2}\right\}}. \tag{29}$$

Proof Let the candidate Lyapunov function $V : \mathbb{D} \to \mathbb{R}$ be defined as

$$V \triangleq \frac{1}{2}e_0^T e_0 + \frac{1}{2}e_1^T e_1 + \frac{1}{2}r^T M_{ST} r, \tag{30}$$

which satisfies the following property as

$$\lambda_1 \|z\|^2 \leq V\left(z\right) \leq \lambda_2 \|z\|^2. \tag{31}$$

where $\lambda_1, \lambda_2 \in \mathbb{R}$ are known positive constants such that $\lambda_1 \triangleq \frac{\min\{1, \underline{m}_{ST}\}}{2}$ and $\lambda_2 \triangleq \frac{\max\{1, \bar{m}_{ST}\}}{2}$. Using (17), (20)-(21) and (26), the time derivative of (30) can be upper bounded as

$$\dot{V} \leq -\left(\alpha_{1min} - \frac{1}{2}\right)\|e_0\|^2 - \left(\alpha_{2min} - \frac{1}{2}\right)\|e_1\|^2 - k_{min}\|r\|^2 + \|r\|\rho\left(\|z\|\right)\|z\| + \|r\|\bar{N}_d + r^T\left(\left(A_a T\right)^T\left(\lambda_c - \lambda_h\right)\right). \tag{32}$$

Remark 5 *When the end-effector does not touch the constraint surface, the force of end-effector is not measured; in other words,* $f_T = A_a^T \lambda_h = 0$. *Using the definition of* A_a *in (11),* $A_a^T \neq 0$ *for all time; therefore, the Lagrange multiplier of holonomic constraint is zero,* $\lambda_h = 0_{c_h \times 1}$. *Since the desired force trajectory is zero when the end-effector does not touch the constraint surface, the control input for force tracking is also zero,* $\lambda_c = 0_{c_h \times 1}$. *In summary, the following property is valid when the end-effector does not touch the constraint surface:*

$$r^T\left(A_a T\right)^T\left(\lambda_h - \lambda_c\right) = 0. \tag{33}$$

While the end-effector is touching the surface, the constrained variable of reduced order model in (14) and its time derivatives are zero as

$$u_2 = \dot{u}_2 = \ddot{u}_2 = 0_{c_h \times 1}. \tag{34}$$

Since the expression in (34) holds while the end-effector is touching the surface, its desired position trajectory and its time derivatives are also zero:

$$u_{d2} = \dot{u}_{d2} = \ddot{u}_{d2} = 0_{c_h \times 1}. \tag{35}$$

Using (34) and (35), the following property can be written while the end-effector is touching the surface:

$$\mu_1 \int_0^t (u_{d2}(\xi) - u_2(\xi))d\xi + \mu_2(u_{d2} - u_2) + \mu_3 (\dot{u}_{d2} - \dot{u}_2) = 0_{c_h \times 1}, \qquad \forall \mu_1, \mu_2, \mu_3 \in \mathbb{R} \tag{36}$$

The auxiliary signal r can be expressed in the form of (36), therefore $r^T (A_a T)^T (\lambda_h - \lambda_c) = 0$. Using (36), the expression in (33) also holds while the end-effector is touching the surface. In summary, while the end-effector whether or not touches the constraint surface; thus, the property in (33) holds, $r^T (A_a T)^T (\lambda_h - \lambda_c) = 0$.

Using (33), completing square the terms $\|r\| \rho(\|z\|) \|z\|$ and $\|r\| \bar{N}_d$ in (32) for r, the following upper bound can be obtained for (32) as

$$\dot{V} \leq -\left(\alpha_{1min} - \frac{1}{2}\right)\|e_0\|^2 - \left(\alpha_{2min} - \frac{1}{2}\right)\|e_1\|^2 - \frac{k_{min}}{2}\|r\|^2 + \frac{\rho^2(\|z\|)\|z\|^2}{k_{min}} + \frac{\bar{N}_d^2}{k_{min}}. \tag{37}$$

Using (29) and (31), the expression in (37) can be upper bounded as

$$\dot{V} \leq -\frac{\min\left\{\left(\alpha_{1min} - \frac{1}{2}\right), \left(\alpha_{2min} - \frac{1}{2}\right), \frac{k_{min}}{2}\right\}}{2\lambda_2} V + \frac{\bar{N}_d^2}{k_{min}}. \tag{38}$$

From (38), $e_0, e_1, r \in \mathcal{L}_\infty$; using (17), $\dot{e}_1 \in \mathcal{L}_\infty$ that implies $\dot{e}_0 \in \mathcal{L}_\infty$. Using (15) and $\dot{e}_0 \in \mathcal{L}_\infty$, is concluded that $u, \dot{u} \in \mathcal{L}_\infty$. Using Assumption 3, the matrices $M_{ST}, C_{ST}, N_{ST}, B_{ST} \in \mathcal{L}_\infty$. Using $u, \dot{u} \in \mathcal{L}_\infty$ and (27), $e_\lambda \in \mathcal{L}_\infty$ that implies $\lambda_c, \lambda_h \in \mathcal{L}_\infty$ and $\tau_f \in \mathcal{L}_\infty$. Since $r, \tau_f, B_{ST} \in \mathcal{L}_\infty$, then $\tau \in \mathcal{L}_\infty$. Since $u, \dot{u}, M_{ST}, C_{ST}, N_{ST}, d_{ST}, B_{ST}, \tau, \lambda_h \in \mathcal{L}_\infty$, then $\ddot{u} \in \mathcal{L}_\infty$. Standard signal chasing algorithms can be utilized to prove that all remaining signals are bounded. □

Remark 6 *The domain, which is arbitrarily large, is defined as* $S_{\mathbb{D}} \triangleq \left\{ z \in \mathbb{R}^{3c_t} \,|\, \|z\| \leq \sqrt{\frac{\lambda_1}{\lambda_2}} \inf \left\{ \rho^{-1}\left(\sqrt{\frac{\sigma k_{min}}{2}}\right)\right\}\right\}$, *where* $\sigma \triangleq \min\left\{\left(\alpha_{1min} - \frac{1}{2}\right), \left(\alpha_{2min} - \frac{1}{2}\right), \frac{k_{min}}{2}\right\}$. *The control gains α_1, α_2 can be chosen large enough, thereby, the control gain k becomes correspondingly larger to satisfy the gain condition in (29). Moreover, choosing the control gain k arbitrarily large results in an arbitrary small ultimate bound for the position tracking error. As choosing the control gain K_λ of force control input as larger, the force tracking error ϵ_λ becomes smaller. In addition to that, increasing the control gains causes rising in the magnitude of the control input; consequently, much more control effort will be needed.*

4. Simulation in Simulink

A numerical simulation is performed to show the performance of the controller in (22)-(24). The mobile manipulator, as illustrated in Figure 1, consists of an RR manipulator and a differential-drive MP, which has two driving wheels and a castor wheel. The position and velocity of the right and left driving wheels are denoted by θ_R, $\dot{\theta}_R$, θ_L, $\dot{\theta}_L$, respectively. The angular position of the first and second joints are symbolized as

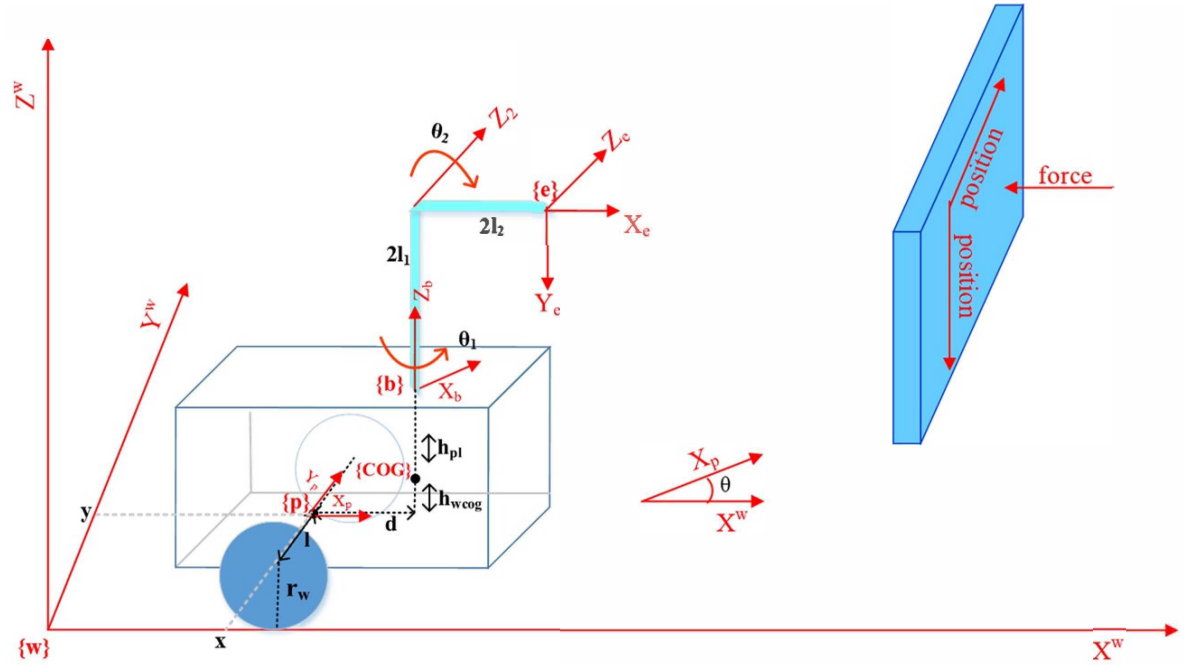

Figure 1. The coordinate systems of the end-effector {e}, the RM base {b}, the MP of the MM {p}, the COG of the MP {COG}, and the world coordinate system {w}.

θ_1 and θ_2, respectively. The length of the first and second links are defined as $2l_1$ and $2l_2$, respectively. The generalized Lagrange coordinates of the MM are given as $q_v=\begin{bmatrix} x & y & \theta \end{bmatrix}^T \in \mathbb{R}^3$ and $q_a=\begin{bmatrix} \theta_1 & \theta_2 \end{bmatrix}^T \in \mathbb{R}^2$. The MP has a nonholonomic constraint due to the structure of its wheels. Considering Assumption 1, the nonholonomic constraint of the MP, which states that the COG of MP moves along the x_p axis and velocity along y_p axis is zero [25], is defined as

$$-\dot{x}s_\theta + \dot{y}c_\theta - d\dot{\theta} = 0, \tag{39}$$

where s_θ and c_θ denote the $sin(\theta)$ and $cos(\theta)$, respectively. The nonholonomic constraint matrix is written as $A_v=\begin{bmatrix} -s_\theta & c_\theta & -d \end{bmatrix}$. The transformation from the generalized Lagrange coordinates to the combined joint-space coordinates of the MP is defined as $\dot{q}_v = S_v\dot{\theta}_v$, where $S_v=\begin{bmatrix} \frac{(r_w c_\theta + d r_w s_\theta/l)}{2} & \frac{(r_w s_\theta - d r_w c_\theta/l)}{2} & \frac{-r_w}{2l} \\ \frac{(r_w c_\theta - d r_w s_\theta/l)}{2} & \frac{(r_w s_\theta + d r_w c_\theta/l)}{2} & \frac{r_w}{2l} \end{bmatrix}^T \in \mathbb{R}^{3\times 2}$, $r_w \in \mathbb{R}$ is the radius of the wheels of the MP, $l \in \mathbb{R}$ is the distance between the COG of the MP and a wheel, $\theta_v=\begin{bmatrix} \theta_L & \theta_R \end{bmatrix}^T$, $\dot{\theta}_v=\begin{bmatrix} \frac{v-l\omega}{r_w} & \frac{v+l\omega}{r_w} \end{bmatrix}^T$, v and w are the linear and angular velocities of the MP [44]. The task space variables of the MM, which are assigned as the position of the end-effector according to the world frame and selected according to the holonomic constraint considering Assumption 4, are defined as X_T and the velocity of the end-effector in the world frame is denoted as $\dot{X}_T$.

$$X_T = \begin{bmatrix} {}^wP_{y_e} \\ {}^wP_{z_e} \\ {}^wP_{x_e} \end{bmatrix} = \begin{bmatrix} y + ds_\theta + 2l_2c_2s_{\theta 1} \\ z + h_{pl} + h_{wcog} + 2l_1 + 2l_2s_2 \\ x + dc_\theta + 2l_2c_2c_{\theta 1} \end{bmatrix}, \qquad \dot{X}_T = \begin{bmatrix} \dot{y} + d\dot{\theta}c_\theta - 2l_2\dot{\theta}_2s_2s_{\theta 1} + 2l_2(\dot{\theta}+\dot{\theta}_1)c_2c_{\theta 1} \\ 2l_2\dot{\theta}_2c_2 \\ \dot{x} - d\dot{\theta}s_\theta - 2l_2\dot{\theta}_2s_2c_{\theta 1} - 2l_2(\dot{\theta}+\dot{\theta}_1)c_2s_{\theta 1} \end{bmatrix}, \tag{40}$$

where $s_{\theta 1}$ and $c_{\theta 1}$ denote the $sin(\theta+\theta_1)$ and $cos(\theta+\theta_1)$, respectively. The RM has a holonomic constraint due to the interaction of the end-effector with a surface. The surface is perpendicular to X^wY^w-plane (or parallel

to Y^wZ^w-plane) and is located at the position $X_{surface}$ on X^w axis. A force in the direction of the X^w axis occurs which includes moving along Y^w and Z^w on this vertical surface. The simulation environment is shown in Figure 1. For touching to surface and moving on it, the X^w axis component of the end-effector's position with respect to {w} should be equal to the position of the surface in X^w axis. In the simulation, we assume that the RM has one holonomic constraint ($c_h = 1$) and the holonomic constraint function is defined as

$$\Theta(X_T) = {}^wP_{x_e} - X_{surface} = 0, \tag{41}$$

and the reduced order variables are selected as u=$\begin{bmatrix} u_1^T & u_2^T \end{bmatrix}^T$ where u_1=$\begin{bmatrix} {}^wP_{y_e} & {}^wP_{z_e} \end{bmatrix}^T$ and u_2=$\begin{bmatrix} {}^wP_{x_e} - X_{surface} \end{bmatrix}$. The transformation matrix $T = I_{3\times3}$, where $I_{3\times3} \in \mathbb{R}^{3\times3}$ is the identity matrix. The desired task is defined in three phases. In the first phase ($t \in [0, T_1)$), the end-effector approaches the surface that is located at a predefined position, and the end-effector tracks a given desired position trajectory. In the next phase ($t \in [T_1, T_2)$), when the end-effector touches the surface, the end-effector tracks both given a desired position and a force trajectories and in the latter phase ($t \in [T_2, T_3]$), the end-effector moves off the surface and the end-effector tracks only a given desired position trajectory. The desired force and position trajectories, which are used to show the performance of the designed controller, are given in Table 3. The desired trajectories imply that when the end-effector is not on the surface, the desired force trajectory equals zero. Thus, only the position of the end-effector needs to be controlled when the end-effector is not on the surface. When the end-effector contacts the surface, a force between the surface and the end-effector along X^w exists. To satisfy the holonomic constraint, the position of the end-effector along X^w should not change while the end-effector moves along Y^w and Z^w axes. Thus, both the force and the position of the end-effector must be controlled during the interaction with the surface.

The matrices of the dynamic model of the MM in (1) was obtained from [44] and the values of the parameters in the MM dynamic are given in Table 4. The parametric disturbances are assumed as m_{1unc}= $0.10m_1sin(3t)$, m_{2unc}=$0.10m_2sin(2t)$, m_{punc}=$0.05m_psin(t)$ and the disturbances in frictions are defined as f_{1unc}=f_{2unc}=$0.01sin(3t)$. The parametric uncertainties ($d_{\Delta_{unc}}(t)$) is constructed with the given parametric disturbances for the simulation and M_{unc}, C_{unc}, and G_{unc} are obtained via substituting the parametric disturbances m_{punc}, m_{1unc}, and m_{2unc} into the m_p, m_1, and m_2, respectively at the matrices in the dynamic model. F_{unc} is obtained via substituting the parametric disturbances f_{1unc} and f_{2unc} into the f_1 and f_2, respectively at the vector in the dynamic model. The disturbance and the friction of MM are assumed as $d_{ext}(t) = [0.05sin(3t)\ 0.025sin(3t)\ 0.04sin(3t)\ 0.05sin(3t)\ 0.1sin(2t)]^T$ and F=$\begin{bmatrix} 0 & 0 & 0 & 0.1\dot{\theta}_1 & 0.1\dot{\theta}_2 \end{bmatrix}$, respectively. The initial conditions of the generalized coordinates of the MM, the initial position of the end-effector and the control gain matrices are given in Table 5. In the simulation, the initial position of the end-effector is selected as 0.15 m error in all axes expressed in $\{w\}$ frame, and the applied control flow diagram for the performed simulation is given in Figure 2. The control strategy of the proposed controller depends on calculating the tracking errors. The tracking errors for position and force are obtained using the desired trajectories and the end-effector's position, velocity, and force. The required measurements (the position, the velocity, and the force measurements of the end-effector) to calculate the tracking errors can be obtained via various sensors in real-time experiments. The calculated input transformation matrix and the tracking errors are used to compute the control input; thereafter, the control input is applied to the actual system for real-time experiments. Although the designed controller does not need the dynamic model of the MM excepting the input transformation matrix, the dynamic model in (14) is utilized to obtain the position, the velocity, and the force of the end-effector for

getting the numerical results.

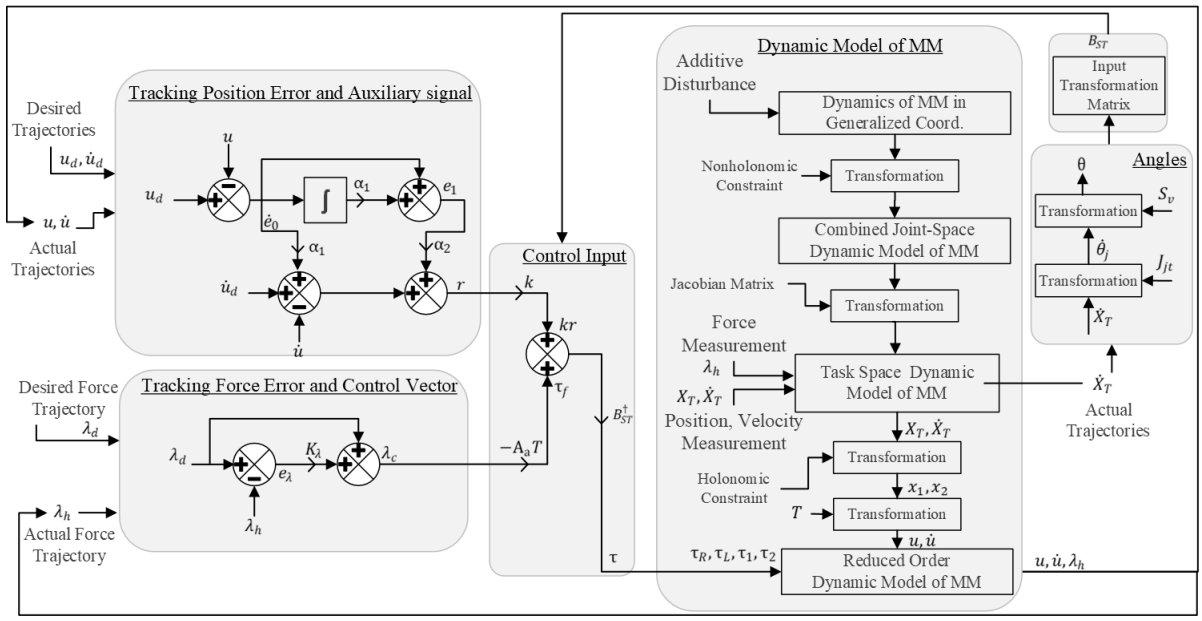

Figure 2. The flow diagram of the designed controller in Simulink.

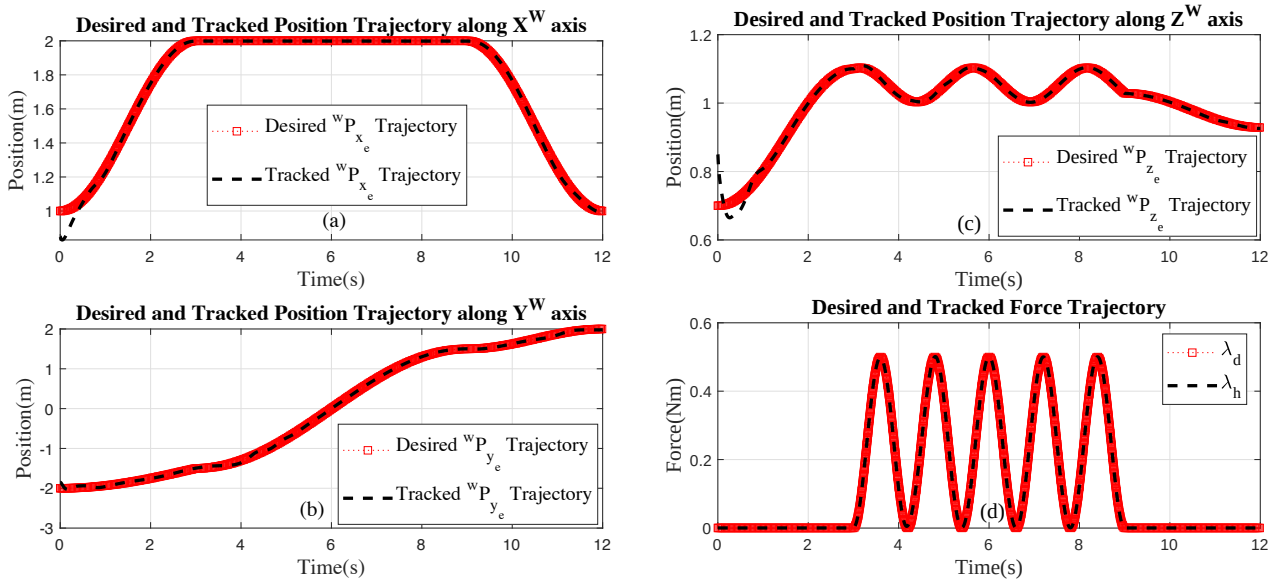

Figure 3. The desired and the actual position of the end-effector along X^w axis in (a), along Y^w axis in (b), along Z^w axis in (c), the desired and the actual force of the end-effector in (d).

The desired and the actual position of the end-effector are shown in Figure 3(a, b, c). In the first 3 s, the end-effector is approaching the surface while it tracks the desired position. Between 3^{rd} and 9^{th} s, the end-effector is moving on the surface and tracks a sinusoidal wave which is the desired position trajectory on the surface. While the end-effector is on the surface, the constrained component of the position of the end-effector has

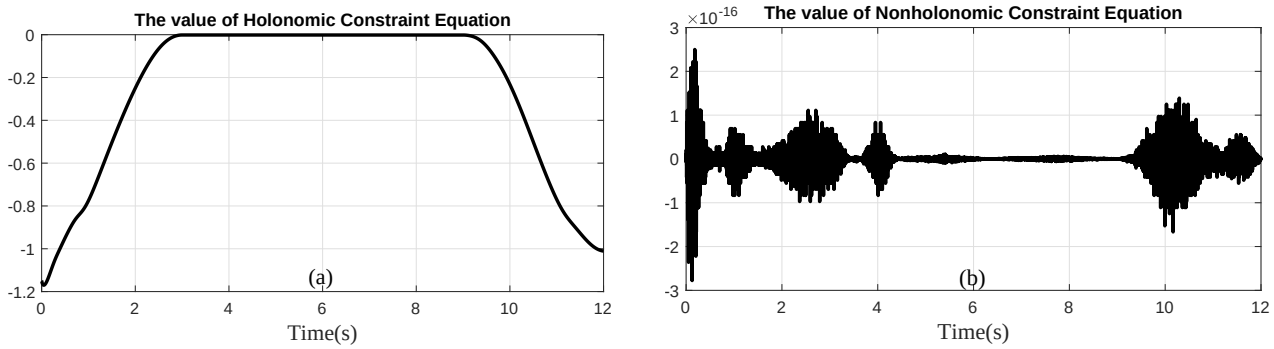

Figure 4. Constraint values, of (a) the holonomic constraint function in (41), (b) the nonholonomic constraint function in (39)

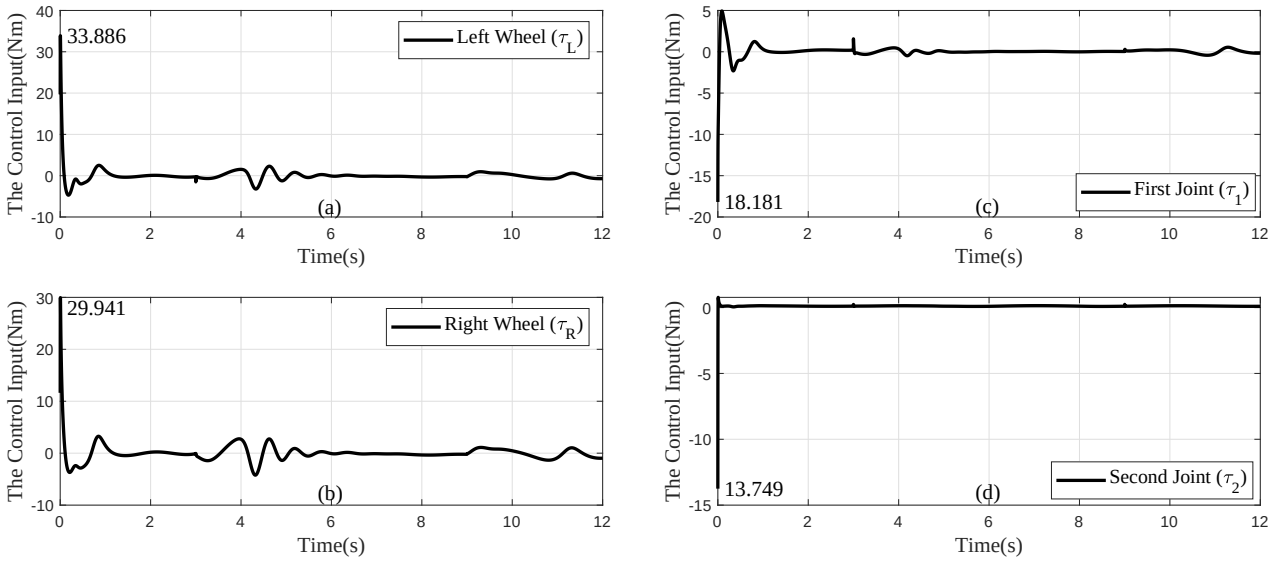

Figure 5. The developed control input, for the left wheel in (a), for the right wheel in (b), for the first joint in (c), for the second joint in (d).

a constant value due to the surface location; however, the unconstrained components provide the desired motion on the surface. In the last period of the simulation, the end-effector is leaving the surface while the end-effector is tracking the desired trajectory. The desired force trajectory is zero while the end-effector is not contacting the surface; however, when the end-effector contacts the surface, the desired force trajectory is sinusoidal. The desired and the actual force trajectories are shown in Figure 3(d). When the interaction starts between the surface and the end-effector, the force control is performed and the maximum absolute error of force tracking is less than 0.017. During the force tracking, the Lagrangian multiplier of the holonomic constraint is calculated by using (14). The value of the holonomic and nonholonomic constraint functions are given in Figure 4. The plot in Figure 4(a) shows that the holonomic constraint function in (41) is satisfied when the end-effector contacts the surface. The value of the nonholonomic constraint is less than 3×10^{-16} for the given desired trajectories as shown in Figure 4(b). The control input (τ) of the MM is shown in Figure 5. The input signals, which include the torque values of the left-right wheels and the joints of the RM, are shown in Figure 5(a, b, c, d). The controller in [24] is

used for comparing the performance of the designed controller. For comparing the performance of the designed controller and the controller in [24], the controllers are used in two different test conditions, and the root mean square errors $\left(RMSE_p \triangleq \sqrt{\frac{\sum_{i=1}^{N=T_3/\Delta t}(u_d-u)^2}{N}}\right.$ for the position, $\left.RMSE_f \triangleq \sqrt{\frac{\sum_{i=1}^{N}(\lambda_d-\lambda_h)^2}{N}}\right)$ for the force, the total variation of control inputs $\left(TV_\tau \triangleq \sum_{i=1}^{N-1}\left|\tau\left(i+1\right)-\tau\left(i\right)\right|\right)$ and the total energy consumption of MM $\left(TEC \triangleq \sum_{i=1}^{N}\left(\sum_{n=1}^{w+k}\left|\tau_n\dot{\theta}_{j_n}\right|\right)\Delta t\right)$ are calculated for both test conditions. The parameters (N) and (Δt) in

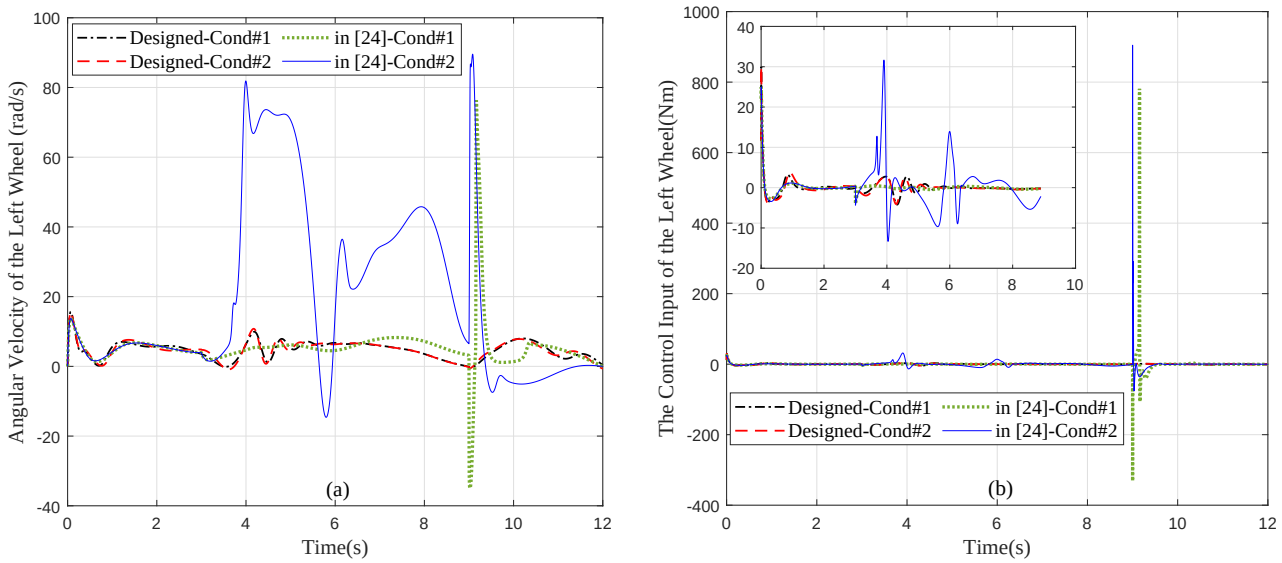

Figure 6. The left wheel's angular velocity in (a) and control input in (b) according to the used controllers (the designed controller and the controller in [24]) in the test conditions.

the performance metrics correspond to the number and the size of the time steps, respectively. The variables (τ_n) and $\left(\dot{\theta}_{j_n}\right)$ in TEC are the torque and the angular velocity of the n^{th} joint of MM, respectively. The test conditions are applied exactly the same to both controllers. In the first and the second conditions, 0.5 and 8 times more additive disturbance was applied to dynamics, respectively. Root mean square of the tracking position error along {w} axes and force tracking error are given in Table 6. The controller in [24] underperforms due to that the control input depends on the dynamics of the MM. However, even though the additive disturbance increases, the designed controller results in less position and force tracking error than the controller in [24]. Furthermore, the total variation of the torque of the left-right wheels and joints of the manipulator is also given in Table 6. The same amount of increase in additive disturbance yields less variation in the designed control input than the controller in [24]. The control input (τ) and the angular velocities $(\dot{\theta}_j)$ of the joints were used to calculate energy consumption, and the results are given in Table 6; moreover, the control input and the angular velocity of the left wheel are shown in Figure 6. As shown in Figure 6(a, b), variations in the control input and angular velocity are much less for the designed controller than the variations resulted for the controller in [24]. The remaining joints of MM show similar behavior. As seen in Table 6, the energy consumption of the proposed method is much less than the energy consumption of the controller in [24]. Additionally, the designed controller provides better performance than the controller in [24] about the energy consumption respect to the additive disturbances.

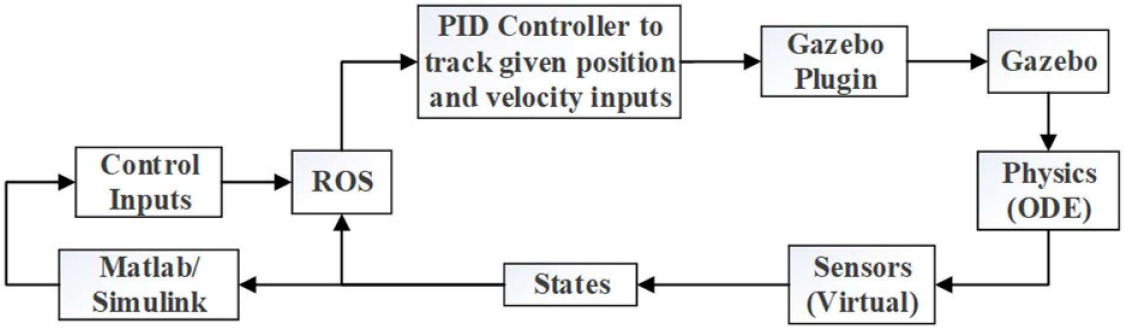

Figure 7. The flow diagram for Gazebo Simulation

5. Simulation in Gazebo

The MM in [44] is constructed for the Gazebo simulation by creating a URDF. The MM has 2 DOF RM and a differential-drive MP. Pioneer 2DX, which is a preexisting differential-drive MP in Gazebo, is used without any change. For the RM, the D-H parameters of the RM in the Simulink simulation are used to prepare the RM's URDF, and the RM is mounted at the center of the Pioneer 2DX [44]. The MP in Gazebo has acceleration limits. The angular acceleration is between $[-3.5, 3.5] rad/s^2$ and the linear acceleration limit is in $[-2.5, 2.5]$ m/s^2. The joints of the RM also have velocity limits. The upper limit of the velocity of the first and second joints of the RM is $20 rad/s$. The transmission interface of each joint selected as "SimpleTransmission" and "DefaultRobotHWSim" is used as the robot simulation type in Gazebo-ROS Control plugin. The hardware interface of the MP and the RM is selected as Velocity and Effort Joint Interfaces, respectively.

The flow of the simulation is given in Figure 7. The simulation in Gazebo[1] cooperates with Simulink and ROS[2] [45]. The differential-drive and Gazebo-ROS control plugins, and a custom plugin that is coded to measure the torques of the MM joints are used to perform the simulation. In the controller part, the position and velocity controllers provided by ROS are used to track the position of the end-effector.

The first stage of the simulation is implementing the position/force controller in Simulink. The implemented controller gives the necessary control inputs (commands) for the Gazebo simulation. These inputs are linear and angular velocities of the MP and the joint angles of the RM. The obtained control inputs were transferred to ROS. The outputs of the PID controller, which is embedded in ROS, are used in the related Gazebo plugins. Finally, the measurements of the position and the heading angle of the MP, the joint positions and the velocities of the wheels, the joint positions and the velocities of the RM, the position, the linear and the angular velocities of the end-effector, the torque of the wheels of the MP and the joints of the RM are obtained from topics of ROS and Gazebo and transferred to MATLAB to compare the Simulink and Gazebo results. In MATLAB, the measurements from Gazebo are used in the designed controller to calculate the torque of each joint in the MM. The calculated and measured torques are compared to show that the designed controller works under the real constraints [46, 47].

The angular velocity of the joints is given in Figure 8. As shown in Figure 8, the measurements from the Gazebo simulation give similar joint velocities as in Simulink. The MP is driven using the angular and the linear velocity of the chassis using a differential drive controller plugin. The MP has limits in most applications

[1]Gazebo (2020). Gazebo Robot Simulator [online]. Website http://gazebosim.org/ [accessed 10 Oct 2020].
[2]ROS (2020). The Robot Operating System [online]. Website https://www.ros.org/ [accessed 10 Oct 2020].

unlike the MP in Simulink; therefore, we applied half of the linear velocity command calculated in Simulink as the linear velocity command in Gazebo. The measurements of the linear and the angular velocities of the MP are given in Figure 9(a, b). The MP has limits on acceleration. Thus, the initial values of the velocities of the MP in Gazebo are different from the data obtained in Simulink. However, the rest of the velocities track the data provided from Simulink. The MP's heading angle and trajectory are given in Figure 9(c, d), respectively. The desired and tracked position trajectories of the end-effector along each axis are given in Figure 10(a, b, c).

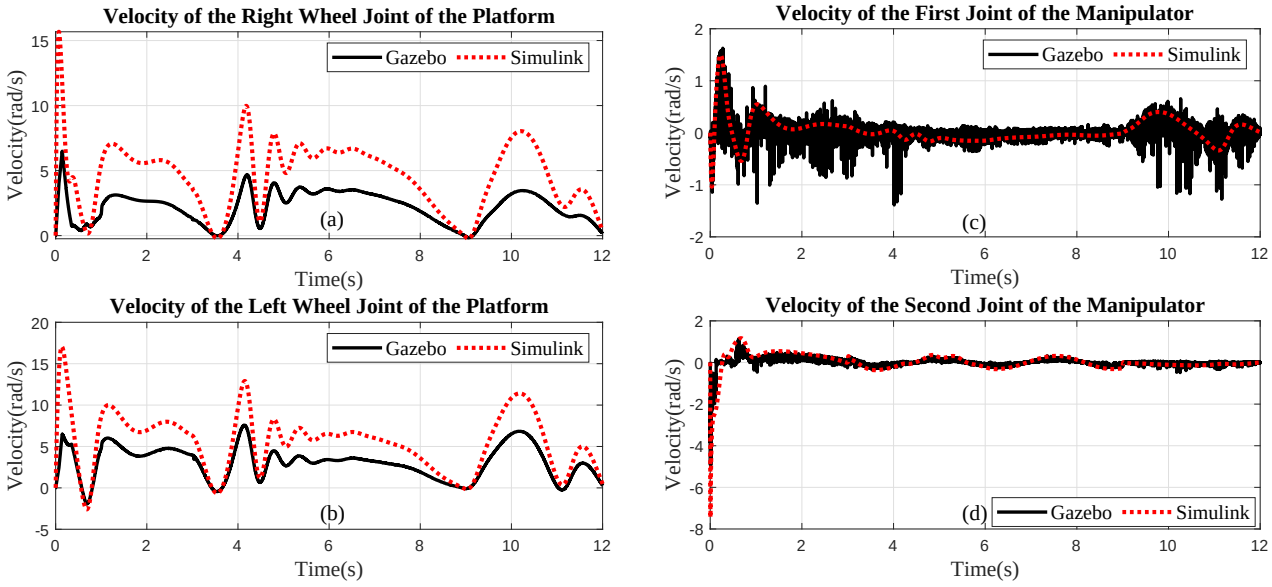

Figure 8. The velocity of the joints from Gazebo Simulation, for the right wheel in (a), for the left wheel in (b), for the first joint in (c), for the second joint in (d)

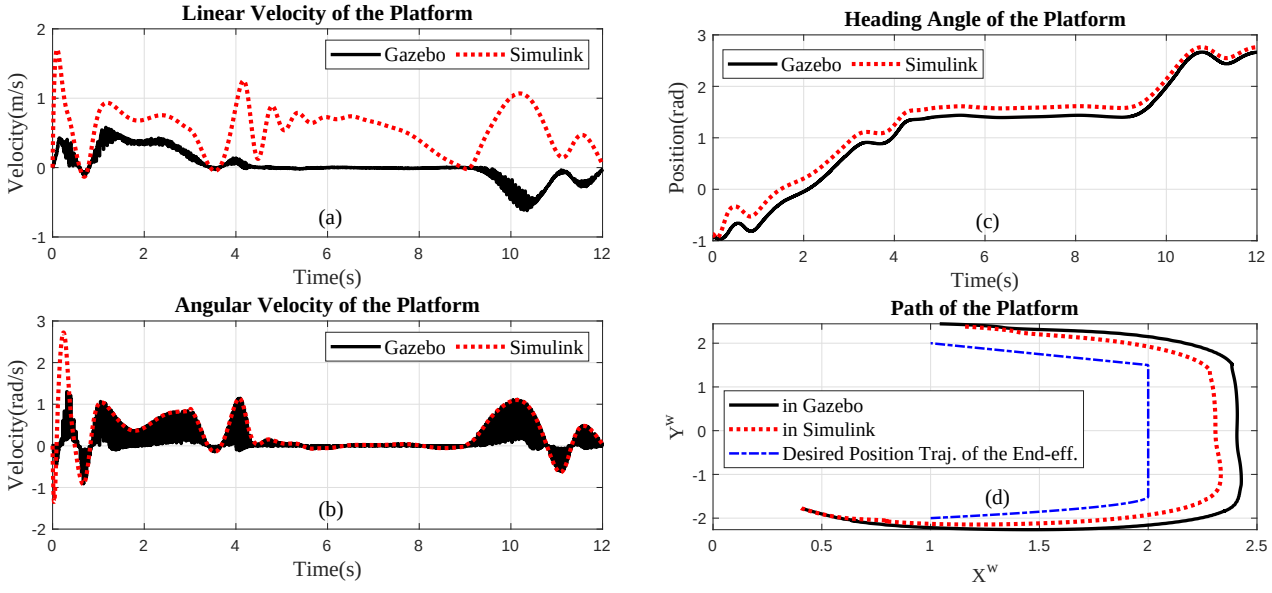

Figure 9. The platform's, linear velocity in (a), angular velocity in (b), heading angle in (c), position in (d) from Gazebo Simulation.

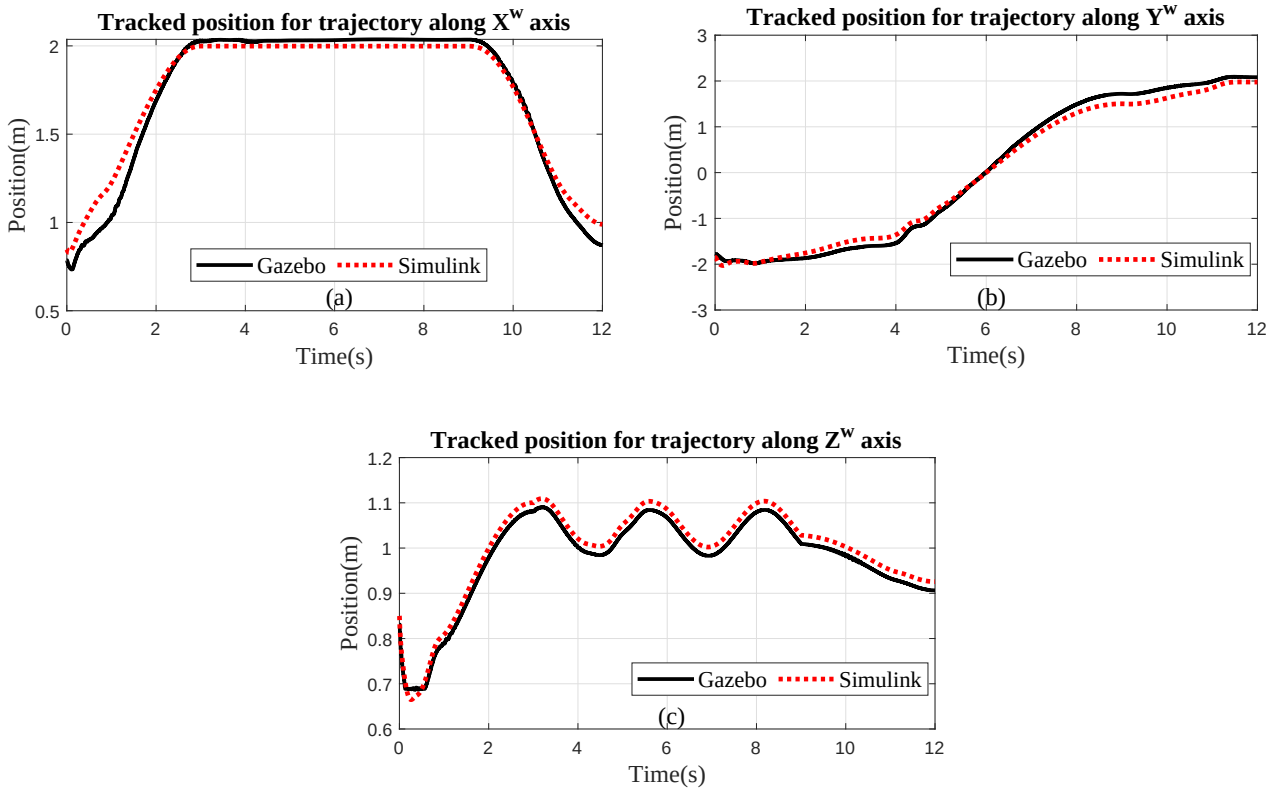

Figure 10. The desired and actual position trajecto-ries in Gazebo Simulation along X^w axis in (a), along Y^w axis in (b), along Z^w axis in (c).

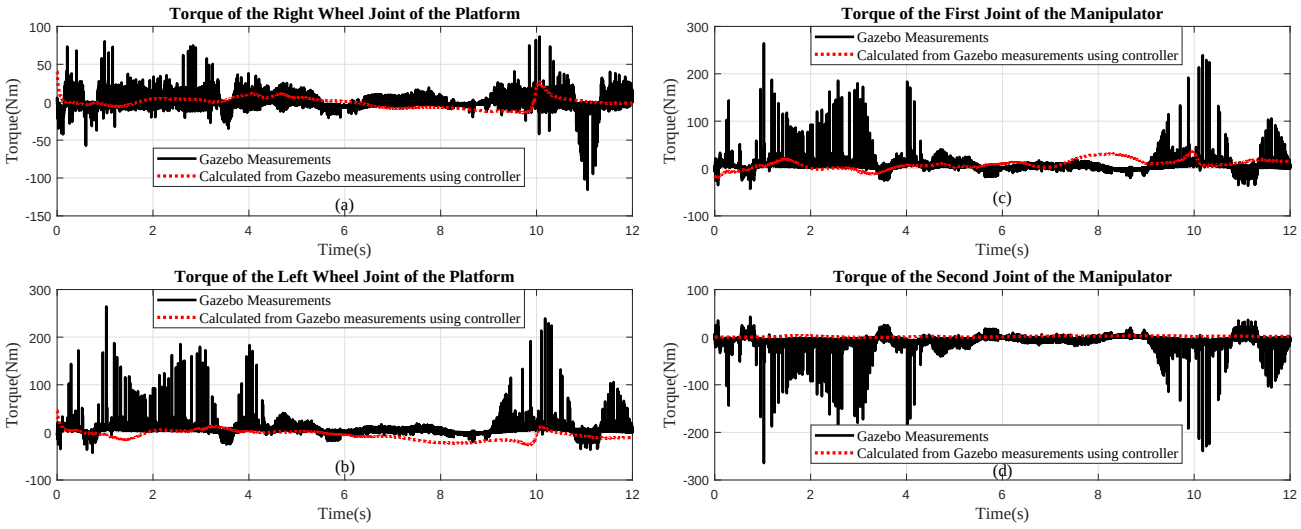

Figure 11. The measured torques and the calculated torques via using Gazebo measurements for tracking the desired trajectory, for the right wheel in (a), for the left wheel in (b), for the first joint in (c), for the second joint in (d).

In Gazebo simulation, the torque of the joints on the MM is measured from a custom Gazebo plugin. To show the performance of the designed controller, the measurements of the MM from Gazebo are used to

calculate the torque of the joints on the MM. The calculated and the measured torques are given in Figure 11(a, b, c, d) for each joint. The torques of the wheels of the MP show a pattern similar to the measured torques. As given in Figure 11, the calculated torques show similarity with the measurements; however, the magnitudes of torques are different than the torques magnitudes from Simulink. Due to the operating PID controllers in ROS are different from the developed controller and the acceleration and velocity limitations on Gazebo, the measured and calculated torques of joints are not exactly the same. However, the desired position and force trajectories are tracked accurately by the MM in both Gazebo and Simulink.

6. Conclusion

In this paper, a robust controller is designed to track the position and the force trajectory for a holonomic constrained nonholonomic mobile manipulator. The uncertainties and disturbances are almost inevitable, and the exact knowledge of the dynamics can not be obtained for the various real-time robotic applications. The designed controller compensates for the effects of the uncertainties in the dynamics and an unknown time-varying additive disturbance while guaranteeing the control objective. Furthermore, the exact knowledge of dynamics and linearly parameterizable assumption are not required for the designed controller. The designed controller ensures that the position and force of the mobile manipulator track their reference trajectories simultaneously even the end-effector touches the constraint surface. Semiglobal uniformly ultimately boundedness of tracking error is proved via Lyapunov-based stability analysis and tracking is achieved to an arbitrarily small neighborhood of the reference trajectories. It might be interesting to consider an unknown time-varying input delay despite uncertainties in the dynamics with an unknown time-varying additive disturbance in future works.

References

[1] Kumar N, Panwar V, Sukavanam N, Sharma SP, Borm JH. Neural network-based nonlinear tracking control of kinematically redundant robot manipulators. Mathematical and Computer Modelling 2011; 53 (9):1889-1901.

[2] Ghajar MH, Keshmiri M, Bahrami J. Neural-network-based robust hybrid force/position controller for a constrained robot manipulator with uncertainties. Transactions of the Institute of Measurement and Control 2018; 40 (5):1625-1636.

[3] Yu L, Fei S, Sun L, Huang J, Yang G. Design of Robust Adaptive Neural Switching Controller for Robotic Manipulators with Uncertainty and Disturbances. Journal of Intelligent and Robotic Systems 2015; 77:571-581.

[4] Braaksma J, Klaassens B, Babuska R, de Keizer C. Hybrid control design for a robot manipulator in a shield tunneling machine. Informatics in Control, Automation and Robotics I 2006; 143-150.

[5] Yim W, Singh SN. Feedback Linearization of Differential-Algebraic Systems and Force and Position Control of Manipulators. In: 1993 American Control Conference; 1993. pp. 2279-2283.

[6] Wei B. Adaptive Control Design and Stability Analysis of Robotic Manipulators. Actuators 2018; 7 (4).

[7] Tuan DM, Hieu PD. Adaptive Position/Force Control for Robot Manipulators Using Force and Velocity Observer. Journal of Electrical Engineering & Technology 2019; 14 (6):2575-2582.

[8] Lozano R, Brogliato B. Adaptive hybrid force-position control for redundant manipulators. IEEE Transactions on Automatic Control 1992; 37 (10):1501-1505.

[9] De Queiroz MS, Hu J, Dawson DM, Burg T, Donepudi SR. Adaptive position/force control of robot manipulators without velocity measurements: theory and experimentation. IEEE Transactions on Systems, Man, and Cybernetics, Part B (Cybernetics) 1997; 27 (5):796-809.

[10] Chwa D. Tracking Control of Differential-Drive Wheeled Mobile Robots Using a Backstepping-Like Feedback Linearization. IEEE Transactions on Systems, Man, and Cybernetics - Part A: Systems and Humans 2010; 40 (6):1285-1295.

[11] Pourboghrat F, Karlsson MP. Adaptive control of dynamic mobile robots with nonholonomic constraints. Computers & Electrical Engineering 2002; 28 (4):241 - 253.

[12] Dixon WE, Dawson DM, Zhang F, Zergeroglu E. Global exponential tracking control of a mobile robot system via a PE condition. IEEE Transactions on Systems, Man, and Cybernetics, Part B (Cybernetics) 2000; 30 (1):129-142.

[13] Fierro R, Lewis FL. Control of a nonholonomic mobile robot using neural networks. IEEE Transactions on Neural Networks 1998; 9 (4):589-600.

[14] Yang JM, Kim JH. Sliding mode control for trajectory tracking of nonholonomic wheeled mobile robots. IEEE Transactions on Robotics and Automation 1999; 15 (3):578-587.

[15] Dixon WE, Dawson DM, Zergeroglu E, Zhang F. Robust tracking and regulation control for mobile robots. International Journal of Robust and Nonlinear Control 2000; 10 (4):199-216.

[16] Venator E, Lee GS, Newman W. Hardware and software architecture of ABBY: An industrial mobile manipulator. In: 2013 IEEE International Conference on Automation Science and Engineering (CASE); 2013. pp. 324-329.

[17] Hvilshøj M, Bøgh S. "Little Helper" — An Autonomous Industrial Mobile Manipulator Concept. International Journal of Advanced Robotic Systems 2011; 8 (2):15.

[18] Engemann H, Du S, Kallweit S, Cönen P, Dawar H. OMNIVIL—An Autonomous Mobile Manipulator for Flexible Production. Sensors 2020; 20 (24):7249.

[19] Hvilshøj M, Bøgh S, Nielsen OS, Madsen O. Autonomous industrial mobile manipulation (AIMM): past, present and future. Industrial Robot: An International Journal 2012.

[20] Yang M, Yang E, Zante RC, Post M, Liu X. Collaborative mobile industrial manipulator: A review of system architecture and applications. In: 2019 25th International Conference on Automation and Computing (ICAC); 2019. pp. 1-6.

[21] Cheng H, Chen H, Liu Y. Object handling using autonomous industrial mobile manipulator. In: 2013 IEEE International Conference on Cyber Technology in Automation, Control and Intelligent Systems; 2013. pp. 36-41.

[22] Zhou K, Ebenhofer G, Eitzinger C, Zimmermann U, Walter C et al. Mobile manipulator is coming to aerospace manufacturing industry. In: 2014 IEEE International Symposium on Robotic and Sensors Environments (ROSE) Proceedings; 2014. pp. 94-99.

[23] Li Z, Ge SS. Fundamentals in Modeling and Control of Mobile Manipulators. CRC Press, 2013.

[24] Kaczmarek M, Domski W, Mazur A. Position-force control of mobile manipulator nonadaptive and adaptive case. Archives of Control Sciences 2017; 27(4):487–503.

[25] Tzafestas SG. Introduction to Mobile Robot Control. Elsevier, 2014.

[26] Tan J, Xi N. Unified model approach for planning and control of mobile manipulators. In: Proceedings 2001 ICRA IEEE International Conference on Robotics and Automation; 2001. volume 3, pp. 3145-3152.

[27] Li Z, Ge S, Adams M, Wijesoma W. Robust adaptive control of uncertain force/motion constrained nonholonomic mobile manipulators. Automatica 2008; 44:776-784.

[28] Li Z, Ge SS, Adams M, Wijesoma WS. Adaptive Robust Output-Feedback Motion/Force Control of Electrically Driven Nonholonomic Mobile Manipulators. IEEE Transactions on Control Systems Technology 2008; 16(6):1308-1315.

[29] Li Z, Ge SS, Ming A. Adaptive Robust Motion/Force Control of Holonomic-Constrained Nonholonomic Mobile Manipulators. IEEE Transactions on Systems, Man, and Cybernetics, Part B (Cybernetics) 2007; 37(3):607-616.

[30] Rani M, Kumar N, Singh HP. Efficient position/force control of constrained mobile manipulators. International Journal of Dynamics and Control 2018; 6:1629–1638.

[31] Kumar N, Rani M. Motion/Force Control for the Constrained Electrically Driven Mobile Manipulators Based on Hybrid Backstepping Control Approach. In: Soft Computing: Theories and Applications. Advances in Intelligent Systems and Computing, Springer, Singapore; 2022. volume 1380 pp. 447-458. doi: doi.org/10.1007/978-981-16-1740-9_36

[32] Makkar C, Hu G, Sawyer WG, Dixon WE. Lyapunov-Based Tracking Control in the Presence of Uncertain Nonlinear Parameterizable Friction. IEEE Transactions on Automatic Control 2007; 52 (10):1988-1994.

[33] Wang ZP, Ge SS, Lee TH. Motion/force control of uncertain constrained nonholonomic mobile manipulator using neural network approximation. In: IEEE Conference on Computer Aided Control System Design; 2006. pp. 2343-2348.

[34] Dawson DM, Lewis FL, Dorsey JF. Robust Force Control of a Robot Manipulator. The International Journal of Robotics Research 1992; 11 (4):312-319.

[35] Yamamoto Y, Yun X. Modeling and compensation of the dynamic interaction of a mobile manipulator. In: Proceedings of the IEEE International Conference on Robotics and Automation; 1994. volume 3, pp. 2187-2192.

[36] Kwan C, Lewis FL, Dawson DM. Robust neural-network control of rigid-link electrically driven robots. IEEE Transactions on Neural Networks 1998; 9 (4):581-588.

[37] Qu Z, Dawson DM, Dorsey JF, Duffie JD. Robust estimation and control of robotic manipulators. Robotica 1995; 13 (3):223-231.

[38] Lewis FL, Dawson DM, Abdallah CT. Robot manipulator control: theory and practice. CRC Press, 2003.

[39] Dixon WE, Behal A, Dawson DM, Nagarkatti SP. Nonlinear Control of Engineering Systems A Lyapunov-Based Approach, Springer, 2003.

[40] Dong W, Huo W. Tracking control of wheeled mobile robots with unknown dynamics. In: Proceedings IEEE International Conference on Robotics and Automation; 1999. volume 4, pp. 2645-2650.

[41] Murray RM, Li Z, Sastry SS. A Mathematical Introduction to Robotic Manipulation. CRC Press, 1994.

[42] McClamroch NH, Wang D. Feedback stabilization and tracking of constrained robots. IEEE Transactions on Automatic Control 1988; 33 (5):419-426.

[43] Dawson DM, Bridges MM, Qu Z, Jamshidi M. Nonlinear Control of Robotic Systems for Environmental Waste and Restoration. Prentice-Hall, Inc., 1995.

[44] Wu Y, Hu Y. Kinematics, dynamics and motion planning of wheeled mobile manipulators. Pro of Int on CSIMTA 2004; 4:221-226.

[45] Doukhi O, Fayjie AR, Lee DJ. Intelligent controller design for quad-rotor stabilization in presence of parameter variations, Journal of Advanced Transportation 2017; 2017.

[46] Zhao B, Tang Y, Wu C, Du W. Vision-based tracking control of quadrotor with backstepping sliding mode control. IEEE Access 2018; 6:72439-72448.

[47] Zhou L, Tzoumas V, Pappas GJ, Tokekar P. Resilient active target tracking with multiple robots. IEEE Robotics and Automation Letters 2018; 4 (1):129-136.

Appendices

A List of abbreviations

Table 1. Explanations of all abbreviations.

Abbreviations	Explanations
MM	Mobile Manipulator
MR	Mobile Robot
RM	Robot Manipulator
MP	Mobile Platform
PID	Proportional Integral Derivative
NN	Neural Network
APDD matrtix	Adjustable, positive definite, diagonal matrix
RR Manipulator	A manipulator which has two revolute joints
COG	Center of gravity
D-H Parameters	Denavit–Hartenberg parameters
URDF	Unified Robot Description Format
$RMSE_p$	Root mean square of position tracking error
$RMSE_f$	Root mean square of force tracking error
TV_τ	Total variation of control input
TEC	Total energy consumption of MM

B Dynamic model in generalized coordinates

Table 2. Submatrices in (1) and explanations.

Submatrices	Explanations
$M_v \in \mathbb{R}^{m\times m}$	Inertia matrices of the MP
$M_a \in \mathbb{R}^{k\times k}$	Inertia matrices of the RM
$M_{av} \in \mathbb{R}^{k\times m}$	the dynamic effect of the MP on the RM
$M_{va} \in \mathbb{R}^{m\times k}$	the effect of the RM motion on the MP
$C_v \in \mathbb{R}^{m\times m}$	The centripetal and Coriolis forces of the MP
$C_a \in \mathbb{R}^{k\times k}$	The centripetal and Coriolis forces of the RM
$C_{av} \in \mathbb{R}^{k\times m}$	The dynamic effect caused by the centripetal and Coriolis forces of the MP on the RM
$C_{va} \in \mathbb{R}^{m\times k}$	The effect of the RM motion on the MP
$N_a \triangleq G_a + F_a \in \mathbb{R}^k$	The gravity and friction of the RM
$N_v \triangleq G_v + F_v \in \mathbb{R}^m$	The gravity and friction of the MP
$d_v \in \mathbb{R}^m$	The additive disturbances for the MP
$d_a \in \mathbb{R}^k$	The additive disturbances for the RM
$B_v \in \mathbb{R}^{m\times w}$	The input transformation matrices of the MP
$B_a \in \mathbb{R}^{k\times k}$	The input transformation matrices of the RM
$\tau_v \triangleq \begin{bmatrix}\tau_L & \tau_R\end{bmatrix}^T \in \mathbb{R}^w$	The torque values of the left and right wheel of MP
$\tau_a \triangleq \begin{bmatrix}\tau_1 & \tau_2 \dots & \tau_k\end{bmatrix}^T \in \mathbb{R}^k$	The torque applied to the joints of RM
$f_n \in \mathbb{R}^m$	The force of nonholonomic constraint
$f_h \in \mathbb{R}^k$	The force of holonomic constraint
$M_{unc} \in \mathbb{R}^{n\times n}$	The inertia matrix of MM due to parametric uncertainties and unmodeled effects
$C_{unc} \in \mathbb{R}^{n\times n}$	The centripetal and Coriolis forces of MM due to parametric uncertainties and unmodeled effects
$G_{unc} \in \mathbb{R}^{n\times n}$	The gravity of MM due to parametric uncertainties and unmodeled effects
$F_{unc} \in \mathbb{R}^{n\times n}$	The friction of MM due to parametric uncertainties and unmodeled effects

C Parameters and Matrices

Table 3. Desired Force and Position Trajectories

		Desired Trajectory
$0 \leq t < T_1$	${}^{w}P_{xd_e}(m)$	$2 - cos((\pi t)/(2T_1))^2$
	${}^{w}P_{yd_e}(m)$	$-1.5 - 0.5cos((\pi t)/(2T_1))^2$
	${}^{w}P_{zd_e}(m)$	$1.1 - 0.4cos((\pi t)/(2T_1))^2$
	$\lambda_d\ (Nm)$	0
$T_1 \leq t < T_2$	${}^{w}P_{xd_e}(m)$	2
	${}^{w}P_{yd_e}(m)$	$1.5 - 3cos((\pi(t - T_1))/(2(T_2 - T_1)))^2$
	${}^{w}P_{zd_e}(m)$	$1.0531 + 0.05sin(2.5t)$
	$\lambda_d\ (Nm)$	$0.5sin((5\pi(t - T_1))/(T_2 - T_1))^2$
$T_2 \leq t < T_3$	${}^{w}P_{xd_e}(m)$	$1 + cos(-\pi(t - T_2)/(2(T_3 - T_2)))^2$
	${}^{w}P_{yd_e}(m)$	$2 - 0.5cos(\pi(t - T_2)/(2(T_3 - T_2)))^2$
	${}^{w}P_{zd_e}(m)$	$0.9287+0.1cos(-\pi(t–T_2)/(2(T_3–T_2)))^2$
	$\lambda_d\ (Nm)$	0

Table 4. Parameters of Dynamic Model of Mobile Manipulator

Parameters	Explanation	Value
$m_{chassis}$,m_p,m_w	Weight of *MP's chassis, the platform, driven wheels*	5.67, 10.57, 1.5 kg
m_1, m_2,m_{sensor}	Weights of *RM*'s links and force sensor	1, 0.55, 0.0075 kg
I_{pxx}, I_{pyy},I_{pzz}	Inertia of *MP*	0.07, 0.08, 0.1 kgm^2
I_{wxx}, I_{wyy},I_{wzz}	Inertia of wheels	0.0051, 0.0051, 0.009 kgm^2
I_{1xx}, I_{1yy},I_{1zz}	Inertia of *RM*'s first link	0.0444, 0.0444, 6.6667e-05 kgm^2
I_{2xx}, I_{2yy},I_{2zz}	Inertia of *RM*'s second link	0.0076, 0.0076, 3.7167e-05 kgm^2
d	Dbtw. the COG and midpoint the wheels	0.1 m
l	Dbtw. the COG and a wheel	0.17 m
r_w	Radius of a wheel	0.11 m
h_{pl}	Dbtw. the *MP*'s COG and top of it	0.05 m
h_{wcog}	Dbtw. the heights of the's COG and wheel axis	0.1 m
$2l_1, 2l_2$	Length of links	0.73, 0.405 m

MP: Mobile platform,*RM*: Manipulator,-*Dbtw.*:-Distance between.

Table 5. Initial conditions and control gain matrices

Initials	Values
$x(0)$	$0.4057\ m$
$y(0)$	$-1.7734\ m$
$z(0)$	$0.16\ m$
$\theta(0)$	$-0.8727\ rad$
$\theta_1(0)$	$0.8727\ rad$
$\theta_2(0)$	$-0.3530\ rad$
${}^wP_{x_e}(0)$	$0.85\ m$
${}^wP_{y_e}(0)$	$-1.85\ m$
${}^wP_{z_e}(0)$	$0.85\ m$
k	$diag(48.6, 37.8, 468)$
K_λ	12250
α_1	$diag\,(0.036, 0.036, 3)$
α_2	$diag\,(28, 71.68, 0.0056)$
Δt	$0.001\ sec$
T_1, T_2, T_3	$3\ sec$, $9\ sec$, $12\ sec$

Table 6. RMSEs, TV and TEC of control input with respect to the designed controller and the controller in [24]

		$RMSE_p$			$RMSE_f$	$TV_\tau(Nm)$				$TEC(J)$
Controller	Condition	along X^w	along Y^w	along Z^w	Force	τ_L	τ_R	τ_1	τ_2	
Designed	1	0.0233	0.0201	0.0109	0.0029	96.633	103.04	46.467	16.16	102.45
in [24]	1	0.4961	0.0751	0.0154	0.1871	2817.3	2540.5	2374.2	67.003	1694.2
Designed	2	0.0294	0.0208	0.0117	0.0036	97.277	104.21	53.871	17.42	104.08
in [24]	2	5.3304	0.0553	0.0172	1.3025	1893	2407.3	1520.6	119.03	2948.2